SOME DETAILED IMPLEMENTATION ASPECTS OF AN AUTOMATED ERROR ASSESSMENT SCHEME FOR ANTENNA SPHERICAL NEAR-FIELD MEASUREMENTS

Patrick Pelland[1], Daniël Janse van Rensburg[2], Derek McNamara[1], Leili Shafai[3]
Shantnu Mishra[3] & Minya Gavrilovic[3]

[1] University of Ottawa, 800 King Edward Ave., Ottawa, Ontario K1N 6N5, Canada
[2] Nearfield Systems Inc., 19730 Magellan Drive, Torrance, CA 90502-1104, USA,
[3] DFL, Canadian Space Agency, 3701 Carling Ave., Kanata, Ontario K2H8S2, Canada.

ABSTRACT

This paper elaborates on certain aspects of a new measurement process that permits an assessment of spherical near-field (SNF) measurement errors based on a set of practical tests that can be done as part of any SNF measurement. It provides error bars for a measured radiation pattern in an automated fashion.

Keywords: Automated Error Assessment, Antenna Pattern Measurements, Spherical Near-Field Testing

1. INTRODUCTION

In [1] the authors described the assessment of spherical near-field (SNF) measurement error[1] based on a set of routine tests. The purpose was to achieve an SNF system that, in an automated fashion, provides error bars for the measured radiation patterns. We identified specific measurement sets that can be done automatically on both an antenna under test (AUT) and the SNF facility, and then used to evaluate the error contributions. The standard 18-term error budget was used as the basis, with some modifications to make it especially relevant to the automated error assessment process. The order in which data sets should be acquired to minimize the overall error assessment time, their relative importance, which ones need be acquired only some of the time and which are AUT-dependent, was described. Finally, [1] also discussed the implementation of such automated error assessment through scripting code.

In the present paper we delve into more detail on some specific implementation aspects of the automated error assessment technique than was possible in [1]. In particular, the results are expanded to a wider treatment of antenna types and frequency ranges. We will assume that the reader has access to [1] since this will allow us to make best use of the available space to include discussions that will be useful to those wishing to apply the method described. Nevertheless Section 2 briefly reviews the automated error assessment process. In Section 3 we provide a catalogue of the three AUT types for which error assessment information is given. Section 4 contains the detailed descriptions of the error terms selected for discussion. Section 5 illustrates how the uncertainty in each direction on the radiation sphere can be displayed as a result of the error assessment procedure described here. Section 6 concludes the paper.

2. AUTOMATED ERROR ASSESSMENT BASICS

The procedure can be briefly reviewed through reference to the actual automated error assessment output interface shown in Fig.1. There are 18 error terms, shown in the lower right hand window in Fig.1, and listed in detail in [1,Table I] and [1,Table II]. A total of six SNF measurements of the AUT, clearly delineated in [1,Table III] and repeated here as Table 1, are performed. Some terminology is explained in Table 2. From these measurements, plus known data that need be determined only once for a given facility and not found anew with each different AUT, the value of each error term can be estimated. These are then combined in a root-sum-of-squares fashion in order to obtain the uncertainty (the error bars) at each pattern angle over the entire radiation sphere surrounding the AUT.

3. AUT TYPES AND OPERATING FREQUENCIES

Table 3 summarizes the three AUTs considered in this paper. The two rightmost columns in the table are for use later in Section 4. The first AUT is the pyramidal horn

[1] It is understood that in the strict sense the term "measurement error" implies an undesired quantity that is quantified and can subsequently be corrected for. The term "measurement uncertainty" implies an undesired quantity that is estimated or bound and cannot be corrected for. In this paper the term "measurement error" is used in reference to both these cases.

antenna in Fig.2. The microstrip patch antenna shown in Fig.3 is different from the horn in that it has a lower directivity and roughly three times the operating frequency. We comment that it was designed as a dual-polarized element [2], but for present purposes we use only the port that provides vertical linear polarization, with the other port terminated. The circularly polarized isoflux antenna shown in Fig.4 was chosen because it has a much higher operating frequency than the other two AUTs, and also because it has a non-standard radiation pattern shape. The above three AUTs have been selected in order to demonstrate the application of the error assessment procedure to several different antenna types and operating frequency ranges.

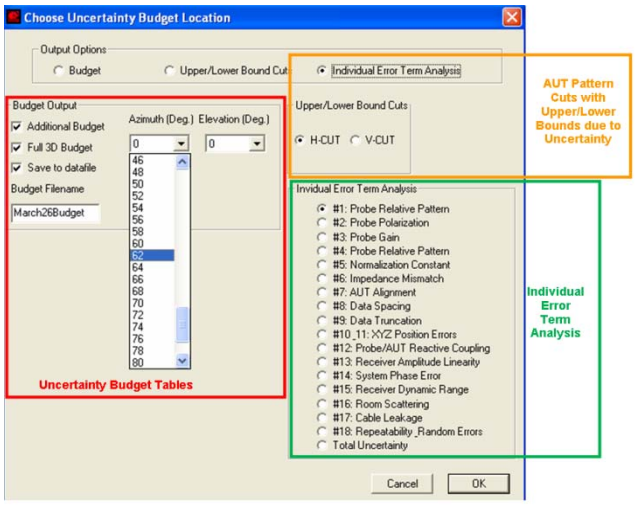

Figure 1 – Automated error analysis output interface.

Table 1 : Numbering of specific measurements

M	Scan Geometry	Details
1	Double Sphere	A redundant theta/phi scan (this means both theta and phi rotate 360 degrees, acquiring two full AUT data sets) taken at slow scan speed with regular density sampling.
1a	180-phi	180-phi data set extracted from M1.
1b	360-phi	360-phi data set extracted from M1.
2	180-Phi	Measurement taken using double density samples.
2a	180-Phi	Single density data set extracted from M2.
3	360-Phi	Record the SNR of the on-axis field measurement.
4	360-Phi	Used for repeatability assessment.
5	-	Rotate the AUT's phi axis and probe axis simultaneously, note the field variation.
6	180-Phi	Measurement taken using a $\lambda/4$ larger sphere radius than all previous measurements.

Table 2 : Some terminology

Terminology	Description
180-phi Scan	Measurement sphere acquired with AUT rotation of $0 \le \Phi \le 180°$, $-180° \le \theta \le 180°$.
360-phi Scan	Measurement sphere acquired with AUT rotation of $0 \le \Phi \le 360°$, $0 \le \theta \le 180°$.
Redundant/Double Sphere	Measurement sphere acquired with $0 \le \Phi \le 360°$, $-180° \le \theta \le 180°$. When averaged, this becomes the "quoted measurement" data. 180-phi and 360-phi data subsets can also be extracted.

Table 3 : Three AUT types considered

AUT	Freq. (GHz)	Directivity (dBi)	SNR (dB)	System Phase Error (dB)
Standard Gain Horn	1.705	14.5	72	0.08
Microstrip Patch	5.5	7.5	52	0.27
Isoflux Horn	14.25	7.0	52	0.20

Figure 2 – Pyramidal horn antenna (EMCO 3160-03 standard gain horn).

4. SOME OUTCOMES OF THE ERROR ASSESSMENT ON SEVERAL ANTENNA TYPES

We have selected five of the eighteen error terms for closer examination. These will next be discussed in turn.

A. Error Term #16 : Room Scattering

In order to quantify the uncertainty associated with room scattering, the approach taken is to compare a redundant scan to a 180-phi or 360-phi scan (the scan types mentioned being defined in Table 2). Since these two measurements will have reflection contributions from different parts of the chamber, a comparison of the two

should yield an ample upper bound to the error associated with room scattering. When choosing the data subset used for comparison (180-phi or 360-phi) with the

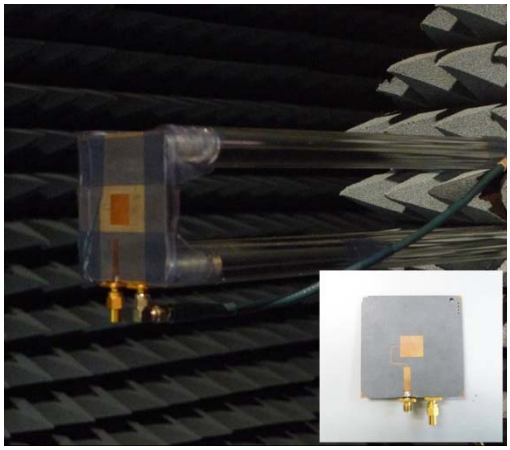

Figure 3 – Mounting of the microstrip antenna in the SNF chamber. Inset shows patch details clearly.

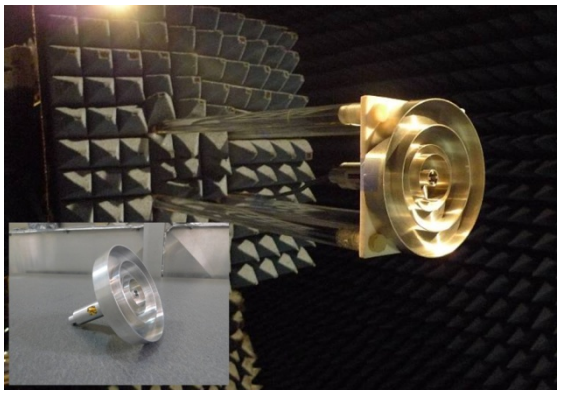

Figure 4 – Mounting of the isoflux antenna in the SNF chamber. Inset shows feed point more clearly.

redundant sphere data, the data acquired using the measurement geometry typically employed in a particular SNF chamber should be selected. In the interest of automation, this method of estimating the uncertainty associated with room scattering has the added benefit of minimizing the number of measurements since the 180-phi or 360-phi data can be extracted from the redundant data set. If a reflection suppression algorithm is available (eg. [3]) this can be used to provide a more precise measure of the error term #16.

In Figs. 5 through 7 we show the error term #16 results for each of the three AUTs. We have kept the same vertical and horizontal axis scales for ease of comparison. In each figure the radiation pattern in red (——) is that obtained using the redundant measurement set from M1. Recall that this measurement is taken at slow scan speed, and so fewer positional errors are expected to be introduced. The 180-phi and 360-phi data sets extracted from this redundant M1 set are averaged, and this tends to "average" out many of the room scattering affects. The black (——) curve is the pattern obtained using extracted data set M1b (see Table 1). The comparison between the two patterns shown provides the associated error signal levels as a function of angle as the blue curve (——). Although specific pattern cuts are shown for purposes of illustration, the method provides such information in all directions over the radiation sphere, as we will show in Section 5.

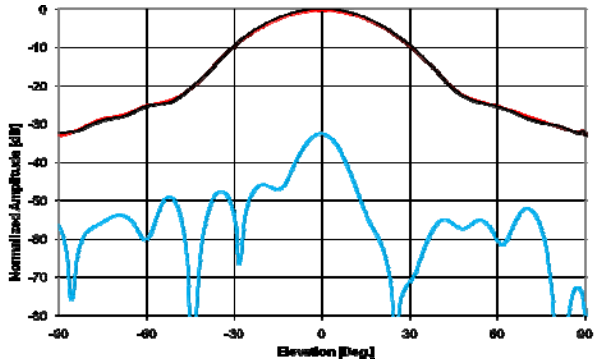

Figure 5 – Error term #16 results for the horn AUT.

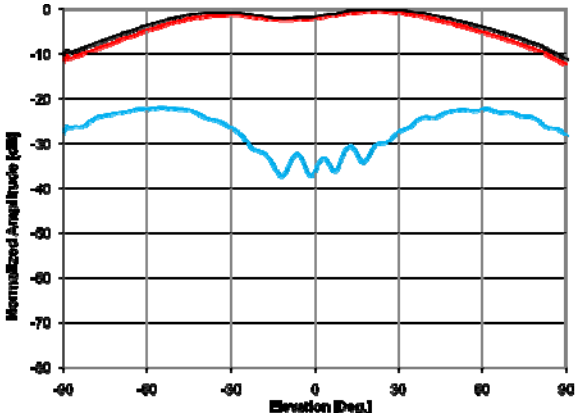

Figure 6 – Error term #16 results for the microstrip patch AUT.

The general higher level of chamber scattering for the lower directivity antennas is evident. It is also worthwhile to note that the errors functions vary significantly as a function of angle, which makes this error term very AUT specific and therefore not easily transferable for a range of AUT's.

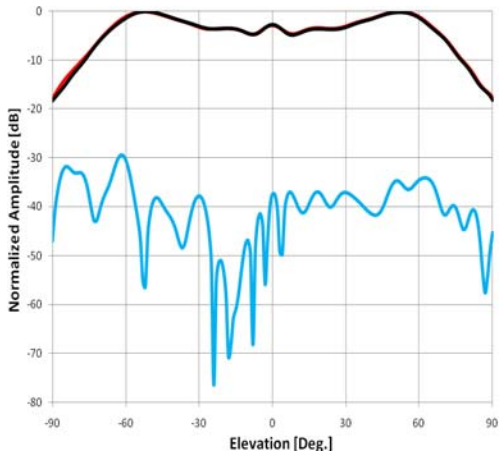

Figure 7 – Error term #16 results for the isoflux AUT.

B. Error Term #17 : Cable Leakage

By disconnecting the cable feeding the AUT and terminating it in a 50Ω load, one can measure a full sphere of cable leakage data across a band of frequencies. By comparing the cable leakage radiation pattern with any of the AUT's radiation patterns (provided they were performed using identical settings) one can quickly determine the error-to-signal ratio and thus measurement uncertainty. As an example, one may wish to measure a 180-phi dataset for a particular AUT. Upon completion, the AUT can be removed, the cable terminated in 50Ω and the 180-phi measurement performed again. These patterns are acquired using identical settings and the difference signal can easily be converted to a measurement uncertainty. This method has the advantage of quoting the most recent and accurate cable leakage uncertainties. However, this option may prove time consuming and unnecessary since this error term is AUT-independent. It requires two user-intervention steps (AUT disconnection and reconnection) and so might be undesirable since it could not be considered to be automated. If this is so the option is to simply apply a full sphere uncertainty profile for cable leakage to a particular AUT's radiation pattern directly from a look-up table. But a cable leakage analysis should then be performed periodically to ensure such look-up tables are up to date.

C. Error Term#14 : System Phase Error

For a spherical near-field test system that contains rotary joints, the most significant contributor to this error term is the amplitude and phase uncertainty introduced by these components. In order to assess the "system phase error" terms for the three AUT types, we record amplitude and phase at the frequency of interest, while rotating the near-field probe polarization axis and AUT phi stage in unison. Normalized amplitude test data for this is shown in Fig. 10. The uncertainty associated with this error is the peak-to-peak value in each case, and so is 0.08 dB for the horn, 0.27 dB for the patch and 0.20 dB for the isoflux antenna. It is important to note that the measurement described here will be affected by range alignment and chamber scattering. We neglect range alignment effects in this instance and the lower measured uncertainty value for the higher directivity AUT (the horn) proves the fact that the result is not only affected by the rotary joints, but also the external scattered signal. The error estimate is therefore a conservative number and we have not attempted to remove any chamber scattering from the results obtained.

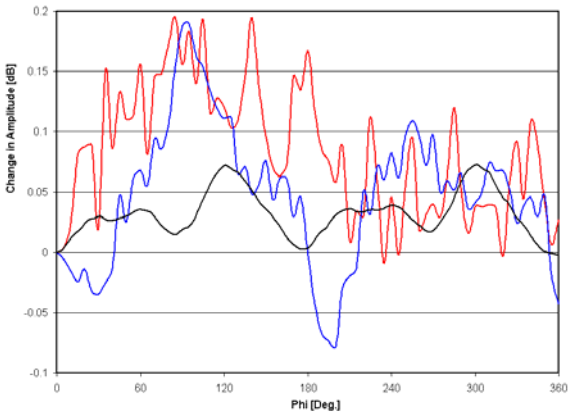

Figure 8 – Normalised amplitude variation for the horn (——), microstrip patch (——) and isoflux (——) antennas.

F. Error Term #12 : Probe/AUT Reactive Coupling

It is well known that in any near-field setup there will inevitably be reactive coupling between the probe and AUT. Therefore, an understanding of the effects of probe/AUT reactive coupling on a measured pattern is required. The approach taken in [4] is to compare two patterns acquired with a λ/4 difference in probe-to-AUT separation. In order to accomplish this, either the AUT or the probe may be shifted. By *increasing* the probe-to-AUT separation, one may be confident that any conditions required regarding the minimum probe-to-AUT separation are still being satisfied. However, one should note that moving either the probe or AUT may introduce additional alignment uncertainties. Since the uncertainty associated with probe alignment is much less severe than that associated with the AUT, the best option is to shift the probe rather than the AUT. However, if a particular chamber does not allow for probe movement, care must be taken when moving the AUT as to not swamp the uncertainty associated with reactive coupling

by AUT alignment uncertainties. Figs. 9 and 10 show the error term #12 results for two of the AUTs under consideration. In each figure the radiation pattern in black (——) is that obtained using the near-field data obtained from M6, whereas that in shown in red (——) is obtained from M2a. The blue curves (——) again show the associated error signal levels as a function of angle in a specific pattern cut.

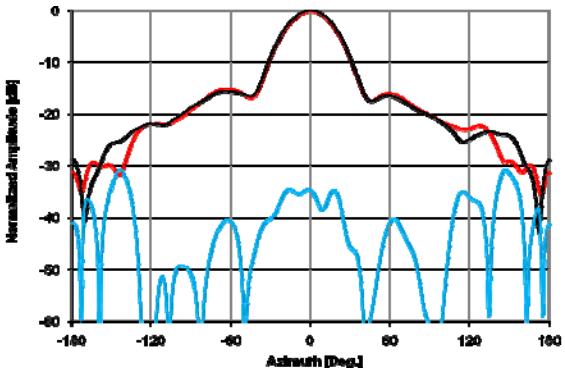

Figure 9 – Error term #12 results for the horn.

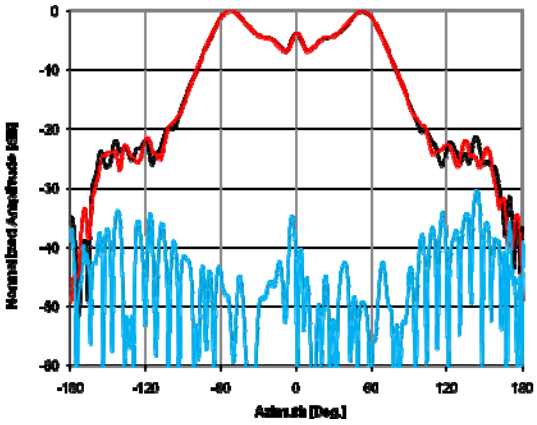

Figure 10 – Error term #12 results for the isoflux AUT.

G. Error Term #13 : Receiver Amplitude Linearity

Fig.11 shows the isoflux radiation pattern with and without receiver amplitude non-linearity correction at the operating band center frequency (14.25 GHz). The correction is performed based on the linearity calibration data of the receiver. Measured amplitude values are adjusted, based on their absolute power levels, and this technique therefore allows one to assess the overall impact of the receiver non-linearity on the measurement.

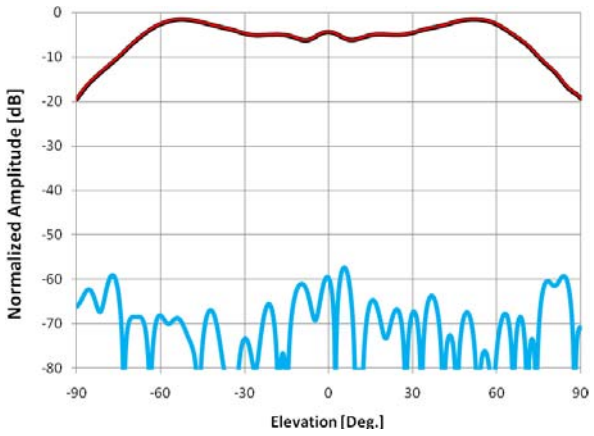

Figure 11 – Isoflux antenna radiation pattern at centre frequency of 14.25 GHz obtained using uncorrected (——) and corrected (——) near-field data. The associated error signal level is shown as (——).

5. PRESENTATION OF RADIATION PATTERN "ERROR BARS"

As stated earlier, the radiation pattern obtained from the averaged 180-phi and 360-phi data sets extracted from M1 is considered to be the "quoted pattern". The overall uncertainty (a combination of all 18 terms) at each pattern angle is then used to quantify the upper and lower bounds, as shown in Fig.12 for the horn AUT (the “blip” on boresight is due to the fact that error terms #3, #5 and #6 apply only at the pattern maximum with respect to which everything else is normalized). The same information over the complete sphere is represented in Figs.13 and 14. The quoted radiation pattern is that in Fig.13.

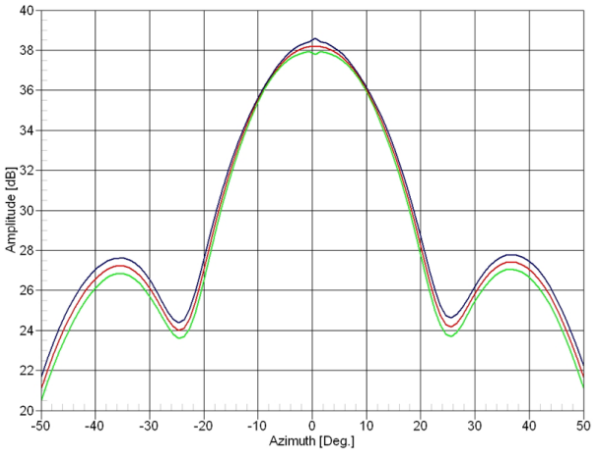

Figure 12 – Quoted radiation pattern (——) along with upper and lower bounds determined from the combined effect of all error terms.

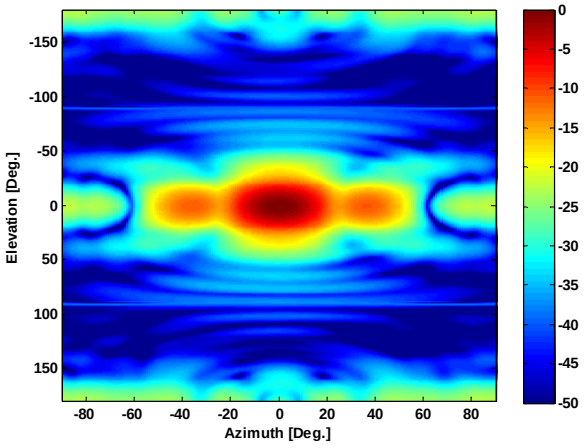

Figure 13 – Quoted normalised radiation pattern.

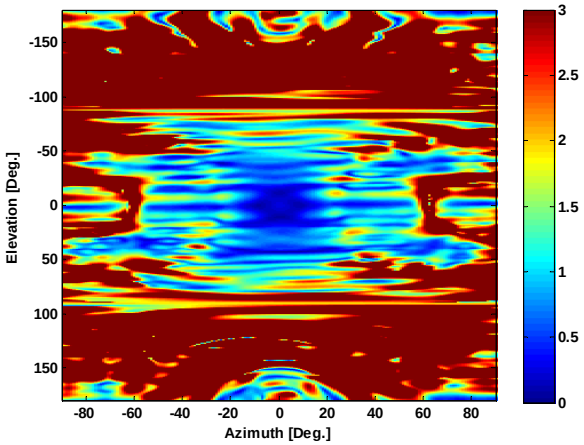

Figure 14 – Associated amplitude uncertainty for each pattern angle over the radiation sphere.

6. CONCLUDING REMARKS

This paper describes an automated error assessment process that has been implemented for use with an SNF antenna test range. The process allows for easy determination of most of the typical errors associated with such types of test systems and presents a first attempt at automation in this sense. Results have been discussed for three different AUT types in order to gain an understanding of how the process works for different antennas. The process also allows for error assessment over the full spherical region of radiation and not only for individual pattern cuts as is often done.

7. REFERENCES

[1] P. Pelland, J. Ethier, D. J. Janse van Rensburg, D. A. McNamara, L. Shafai & S. Mishra, "Towards Routine Automated Error Assessment in Antenna Spherical Near-Field Measurements", Proc. 4th European Conf. Antennas & Propagation (*EuCAP 2010*), April 2010, Barcelona, Spain.

[2] I. Acimovic, D. A. McNamara & A. Petosa, "Dual-Polarized Microstrip Patch Planar Array Antennas with Improved Port-to-Port Isolation", *IEEE Trans. Antennas & Propagation*, Vol.56, No.11, pp.3433-3439, Nov. 2008.

[3] G. Hindman & A. Newell, "Mathematical Absorber Reflection Suppression (MARS) for Anechoic Chamber Evaluation and Improvement", Proc. Antenna Measurement Techniques Association (*AMTA*) Annual Symp., 2008.

[4] G. Hindman, A. Newell, "Simplified Spherical Near-Field Accuracy Assessment", Proc. Antenna Measurement Techniques Association (*AMTA*) Annual Symp., 2006.